ACS APPLIED MATERIALS & INTERFACES

Research Article

www.acsami.org

Electrical Resistivity of Assembled Transparent Inorganic Oxide Nanoparticle Thin Layers: Influence of Silica, Insulating Impurities, and Surfactant Layer Thickness

Stephanie B. Bubenhofer,[†] Christoph M. Schumacher,[†] Fabian M. Koehler,[†] Norman A. Luechinger,[†] Georgios A. Sotiriou,[‡] Robert N. Grass,[†] and Wendelin J. Stark*,[†]

[†]Functional Materials Laboratory, Institute for Chemical and Bioengineering, ETH Zurich, CH-8093 Zurich, Switzerland

[‡]Particle Technology Laboratory, Institute of Process Engineering, ETH Zurich, CH-8092 Zurich, Switzerland

S *Supporting Information*

ABSTRACT: The electrical properties of transparent, conductive layers prepared from nanoparticle dispersions of doped oxides are highly sensitive to impurities. Production of cost-effective thin conducting films for consumer electronics often employs wet processing such as spin and/or dip coating of surfactant-stabilized nanoparticle dispersions. This inherently results in entrainment of organic and inorganic impurities into the conducting layer leading to largely varying electrical conductivity. Therefore, this study provides a systematic investigation on the effect of insulating surfactants, small organic molecules and silica in terms of pressure dependent electrical resistivity as a result of different core/shell structures (layer thickness). Application of high temperature flame synthesis gives access to antimony-doped tin oxide (ATO) nanoparticles with high purity. This well-defined starting material was then subjected to representative film preparation processes using organic additives. In addition ATO nanoparticles were prepared with a homogeneous inorganic silica layer (silica layer thickness from 0.7 to 2 nm). Testing both organic and inorganic shell materials for the electronic transport through the nanoparticle composite allowed a systematic study on the influence of surface adsorbates (e.g., organic, insulating materials on the conducting nanoparticle's surface) in comparison to well-known insulators such as silica. Insulating impurities or shells revealed a dominant influence of a tunneling effect on the overall layer resistance. Mechanical relaxation phenomena were found for 2 nm insulating shells for both large polymer surfactants and (inorganic) SiO_2 shells.

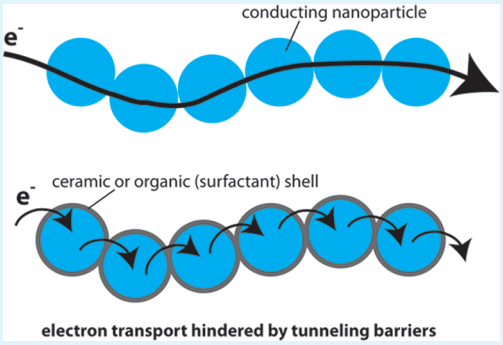

KEYWORDS: *conductive oxides, antimony tin oxide, charge transport, core–shell nanocrystals, thin films*

INTRODUCTION

In the last decades, transparent conductive oxides (TCO) have gained more and more importance in electrical devices: Thin films of the highly conductive oxidic materials are used as top electrode materials in solar cells, liquid crystal displays, and light emitting diodes.[1−3] Beside their transparency and conductivity, they reflect thermal infrared heat,[2,4−6] which is an advantage for most of the above-mentioned applications as well as for future use as low-energy windows.

Among the different TCO materials, indium tin oxide (ITO) is the best-known composition. It exhibits a high electrical conductivity combined with high light transmission. However, the rare occurrence of indium on earth[7,8] demands the search for other doping materials of tin and zinc oxides. Antimony, aluminum and fluorine are heavily investigated and a balance between optimal performance and abundance/cost has to be found.[3,4,9−14]

Vacuum deposition methods such as sputtering and CVD are the most common to produce traditional polycrystalline films of different oxide materials[15−18] on rigid substrates as for example glass. Scale up processes and cost reduction of electronic devices as well as the growing interest in producing flexible electrodes on polymer substrates lead to a focus on new film production methods.[19−21] This technical challenges demand improvements in low temperature processing of transparent conductive oxide films.[22−24] Sol–gel routes, spray pyrolysis as well as spin and dip coating or even printing of TCO-nanoparticle solutions have been investigated and show promising results for cheap transparent conducting layers.[25−29]

For these economically interesting coating processes of thin nanoparticle films, wetting agents or functionalization of the particles are often necessary to prohibit the aggregation of the nanoparticles during the processing steps and to provide proper film formation properties.[30−32] These surfactant- and functionalization molecules play a tremendous role in the performance of nanoparticle assemblies.[33,34] The electrical conductance, however, can be seriously affected by an adsorbate shell around the particles, especially when low-temperature processing is

Received: February 23, 2012
Accepted: April 30, 2012
Published: April 30, 2012

needed for flexible devices, where no heat treatment is possible to remove the organic materials (sensitive polymer substrates). Therefore, it is necessary to deal with the impact (positive and negative) of those organic impurities. As shown by Maksimenko et al.[35] additives as polyvinylpyrrolidone (PVP) can even enhance the conductivity of TCO thin films due to shrinkage in the drying process. Several studies focused on understanding the influence of molecules,[36,37] polymers[38−40] and insulating barriers on the conductivity in nanoparticle composites. Models for percolation and hopping of electrons through nanoparticle assemblies have been investigated.[41] Moreover, tunneling of electrons through thin insulating shells or filler materials in a nanocomposite play an important role.[42] However, these reports have shown a considerable spread of data and various explanations for the electron transport in shells.

In the present study we, therefore, attempt to present systematic investigations on how insulating shells on TCO nanoparticles influence the overall resistivity of assembled nanoparticle thin films. High temperature derived antimony tin oxide (ATO) nanoparticles (guaranteed no adsorbed organics) were optionally coated with different dispersing agents or directly produced as SiO_2 coated ATO particles (one step coating and production process). Flame spray synthesis allowed a controlled antimony dopant level[43] in ATO and the in situ deposition of a SiO_2 shells with a well-controlled thickness.[44] The organic coatings were fabricated by drying different surfactant-stabilized dispersions of flame derived ATO nanoparticles. Using a systematic study on pressure dependent resistance allowed us to investigate the accurate role of shell thickness and mean conducting core distance between nanoparticles on the overall resistivity in the nanoparticle assembly.

EXPERIMENTAL METHODS

Materials. 2-(2-(2-Methoxyethoxy)ethoxy)acetic acid (TODA) and Tin(II) 2-ethylhexanoate (~95%) were purchased from Aldrich Fine Chemicals. Ethanol absolute (analytical grade, ACS) was purchased from Scharlau (Scharlab S.L.), ethylene glycol from Acros Organics and tetrahydrofuran (HPLC grade) from Fisher Scientific. DISPERBYK-2164 was supplied by BYK-Chemie GmbH. Antimony-(III) n-butoxide was purchased from ABCR-Chemicals. Technical grade xylene and 2-ethylhexanoic acid were used.

ATO Particle Synthesis. The antimony tin oxide particles (10 wt % antimony in SnO_2) were synthesized by an enclosed single step flame spray pyrolysis (FSP) setup. In analogy to the setup for the reducing flame synthesis according to Grass et al.[45] a hermetically sealed glovebox including the flame spray setup was built (3-glove-system, GS GLOVEBOX Systemtechnik GmbH). The glovebox is operated with an air at atmospheric conditions and protects the environment from nanoparticle exposure. The multicomponent precursor was prepared by mixing defined amounts of Sb(III) n-butoxide and Tin(II) 2-ethylhexanoate in 2-ethylhexanoic acid.[46] The precursor was diluted with THF (2:1) and had a total metal concentration of 4 wt %. The precursor was then dispersed (5 L min^{-1} O_2, 5 mL min^{-1} liquid) by a nozzle into a premixed flame (2.4 L min^{-1} O_2, 1.13 L min^{-1} CH_4) operated in the glovebox. In the off gas above the flame, the nanoparticles were collected with a glass fiber filter (Whatman GF/A, 25.7 cm diameter, within the glovebox). A detailed description of a similar flame spray setup (without enclosure) is given by Maedler et al.[47]

Organic Functionalization. To functionalize the as-prepared particles, dispersions of 5 wt % particles were made by Nanograde LLC in a variety of solvents: The ethylene glycol functionalization was made with pure ethylene glycol (EG). To functionalize the particles with 3,6,9-trioxadecanoic acid (TODA), we used ethanol as solvent, and for the polymer functionalization, DISPERBYK-2164 (polymer) is taken as surfactant and xylene as solvent.

Synthesis of Silica-Coated ATO Particles. Silica-coated ATO-particles were prepared in a slightly different enclosed flame spray pyrolysis reactor.[48] The same ATO-precursor as for the production of pure ATO-particles was dispersed by 5 L min^{-1} oxygen into a 1.5 L min^{-1}/3.2 L min^{-1} methane/oxygen flame. Additionally, sheath gas (40 L min^{-1} O_2) surrounding the flame was also provided to ensure complete combustion. The flame was enclosed by a 20 cm quartz glass tube, on top of which a metallic ring with 16 equidistant openings was placed. Through these openings, hexamethyldisiloxane (HMDSO, Sigma-Aldrich, purity >98%) vapor was injected along with 15 L min^{-1} N_2 carrier gas. The HMDSO vapor was supplied by bubbling N_2 at appropriate flow rates through a HMDSO containing flask. The reactor was terminated by a 30 cm quartz glass tube.

Particle Analysis. Transmission electron microscopy (TEM) images of the pure and SiO_2-coated particles (not shown) were made utilizing a FEI Tecnai F30 microscope (FEG cathode, operated at 300 kV, point resolution ~2 Å). The particle size as well as the SiO_2-shell thickness was determined from these images (log-normal fitting, 1 nm step). X-ray diffraction patterns were recorded on a X'Pert PRO-MPD (Cu Kα radiation, X'Celerator linear detector system, step size of 0.05°, 45 kV, 40 mA, ambient conditions) and the as-prepared particle size was calculated by the Debey-Scherrer-equation.[49] Nitrogen adsorption measurements of the inorganic particles were performed (Brunauer−Emmett−Teller (BET) method, Tristar Micromeritics Instruments) following a sample pretreatment of 3 h at 140 °C under vacuum. Thermogravimetrical analysis (see the Supporting Information, Figure 1) was made to determine the organic content (functionalized-shell) on a TG STAPT1600 (Linseis) with a heating rate of 10 °C min^{-1} under air up to 800 °C. The shell thickness of the organic/ATO composites was calculated from the following geometric consideration, assuming spherical particles and a density of the organic phase of 1 g cm^{-3}:

$$\frac{V_{shell}}{V_{core}} = \frac{V_{total} - V_{core}}{V_{core}} = \frac{\frac{4}{3}\pi(r_{core} + x)^3 - \frac{4}{3}\pi r_{core}^3}{\frac{4}{3}\pi r_{core}^3} = \frac{(r_{core} + x)^3 - r_{core}^3}{r_{core}^3} = \frac{m_{shell}}{m_{core}}\frac{\rho_{core}}{\rho_{shell}}$$

where V denotes the volume, r the radius, m the mass and ρ the density of either the core or the shell material. x is the shell thickness, which can then be calculated from the mass ratio gained from the thermogravimetrical analysis. This procedure is in line with the strong, irreversible adsorption of surfactants and polymer monolayers.[50,51] For the polymer/ATO composite, the volume content of polymer is high and we can additionally assume that all interparticle voids are filled with polymer. Because the packing is clearly random, a volume filling ψ = 0.5 can be assumed as generally accepted in powder technology[52] and affords a smaller shell thickness of 0.8 nm (see the Supporting Information, Figure 2, for details).

Resistivity Measurements. The resistance of the pestled powder was measured by a two-point measurement between to hardened stainless steel cylinders (about 0.3 Ohm wiring and contact resistance) under different pressures at a constant current with a Keithley Series 2400 SourceMeter (measurements were 10 s after pressure stabilization). The pressure was applied by manually compacting the powder in an uniaxial press (IR-Presse-25T, manual, hydraulic, Maassen GmbH). The thickness of the pill was determined either by an optical microscope (Zeiss, Axio Imager.M2m, z-stacking) or by a caliper (Sylvac, S_Cal Work).

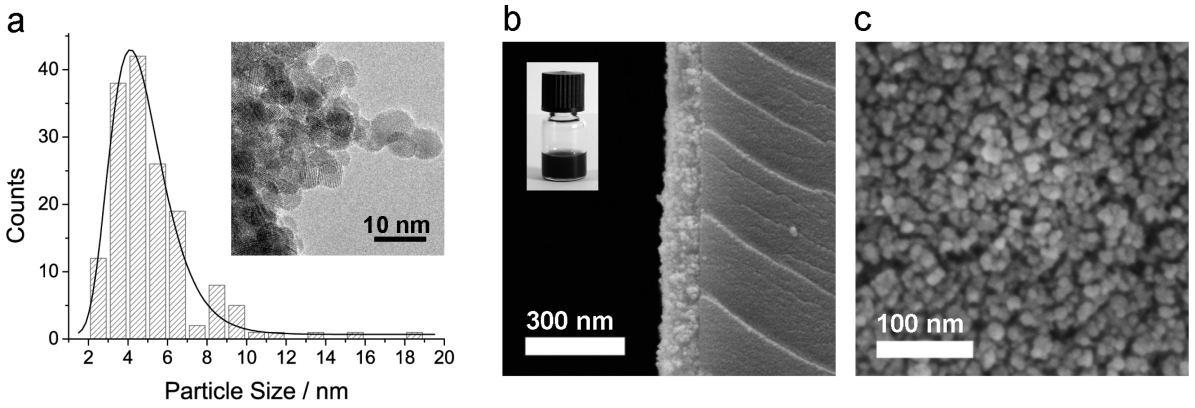

Figure 1. (a) Particle size distribution of antimony-doped tin oxide (ATO) nanoparticles after preparation with a log-normal curve fit and representative electron micrograph. (b) Dispersion containing 5 wt % ATO (polymer−surfactant) in xylene and resulting spin-coated thin film (cross-section) and (c) top view.

RESULTS AND DISCUSSION

Nanomaterial Dispersions and Film Preparation. Antimony tin oxide (ATO) nanoparticles with an antimony (Sb) content of 10 wt % were prepared by flame spray synthesis. This high-temperature preparation method has routinely been used for oxide preparation with high purity (high temperature results in destruction of organic surface impurities).[53−55] The as-prepared pure ATO nanoparticles were characterized with complementary methods and showed a log-normal primary particle size distribution (mean 4.5 nm, σ_g = 1.35) and an average diameter of 5.2 ± 2.3 nm (157 particles optically counted using transmission electron microscopy images; Figure 1a). Specific surface area measurements according to the BET method revealed a surface area of 124 $m^2\ g^{-1}$ (Table 1) which results in a surface-equivalent particle diameter of 7.1 nm if assuming spherical particles and a density of 6.8 g cm^{-3} for the antimony tin oxide.[45] X-ray diffraction patterns of the material confirmed its chemical identity (match of crystal phase to literature data) and yielded a mean crystallite diameter of 6.9 nm (applying the Debye−Scherrer equation on the main reflection peak). These measurements confirmed the optical (electron microscopy) characterization of the material and showed that it consists of about 7 nm, rather single-crystalline particles of ATO. For mechanistic investigations a series of SiO_2 coated ATO nanoparticles with different shell thicknesses (nominal values: 0.7, 1.4, 2.1, and 2.8 nm; calculated by assuming shells around monodisperse spheres (core diameter from uncoated particles from BET)) were prepared using a modified flame spray synthesis setup[48] where a gaseous Si-precursor vapor was injected further downstream of the freshly formed core ATO-nanoparticles at a height of 20 cm. The flame was surrounded by a glass tube to provide a better turbulent flow mixing of the different components[56] and to inhibit air entrainment in the reactor.

Table 1. Summary of BET Analysis and Shell Thickness Measurements by TEM and Thermogravimetrical Analysis

	material	specific surface area from BET ($m^2\ g^{-1}$)[c]	shell thickness (nm)
series 1	ATO (enclosed FSP−setup)	124	
	ATO−polymer		2[a]
	ATO−EG		0.7[a]
	ATO−TODA		0.7[a]
series 2	ATO (SiO_2−FSP−setup)	38	
	ATO−0.7 nm SiO_2	42	
	ATO−1.4 nm SiO_2	47	1.7[b]
	ATO−2.1 nm SiO_2	59	1.9[b]
	ATO−2.8 nm SiO_2	66	2.1[b]

[a]Shell thickness determined by geometrical considerations from thermogravimetrical analysis data. [b]Shell thickness determined by TEM image analysis. [c]Specific surface area error: ± 5%

High-quality dispersions are needed to inhibit aggregate formation during processing as spin- or dip-coating since such premature aggregate formation results in film inhomogeneity, rupture, or holes. As known from colloid science, stabilization of small particles in a fluid can either be done electrostatically or sterically.[57] Steric stabilization is usually performed by adding (bulky) surfactants to the fluid or by chemically functionalizing the particles. In both cases, a spacer is introduced between the particles thus reducing their attractive force. High quality nanoparticle dispersions are the key requirement to form good, conducting films and today mainly rely on certain optimized, organic additives (usually rather high molecular weight compounds). After film formation and evaporation of the solvent, the stabilizing agents remain in the nanoparticle film. These insulating (nonconducting) surfactants are traditionally removed by annealing the films under high temperature which may also induce a usually beneficial side-effect, namely sintering, which maximizes the contact area between adjacent particles and improves conductivity. The now ongoing transformation to flexible (usually polymer-based) film substrates, however, severely limits the application of such high-temperature post-treatments. Surfactant removal, hence, has become more difficult and demands for alternative film preparation strategies.

To better understand the effect of such insulating additives, a number of samples with varying contents and size of commercially used surfactants were prepared and compared to assembled ATO nanoparticles without any additives (e.g., absence of impurities as far as technically possible). Dispersions with 5 wt % ATO were either stabilized by a polyurethane-based dispersion additive (polymer) and supplied in xylene (sample a, i.e., the thickest coating) or using a small molecular surface modifier, trioxadecanoic acid (TODA) and supplied in ethanol (b) or prepared without additional surfactants (c) in ethylene glycol (EG) where a direct adsorption of ethylene

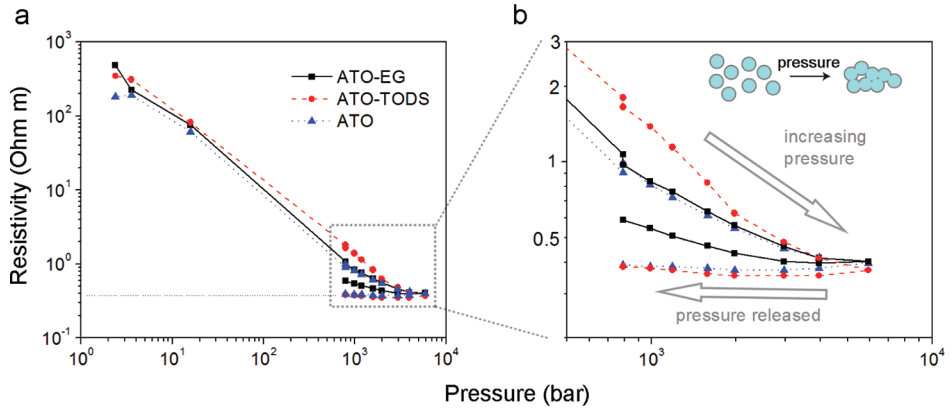

Figure 2. (a) Electrical resistivity of compacted ATO nanoparticles under various pressures and using different organic additives with increasing size and (b) detailed view on the behavior at high pressures. All samples undergo an irreversible compaction and maintain a decreased resistivity after pressure release.

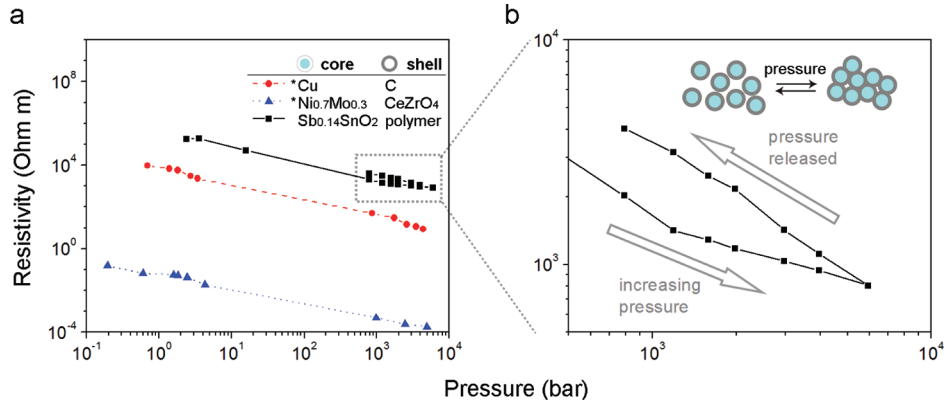

Figure 3. (a) Electrical resistivity of compacted ATO particles using a polymeric additive as dispersion agent (top series of data) and comparison to literature data on 1−3 nm ceramic-coated metal core/shell nanoparticles (bottom data) and insulating 1 nm carbon coated copper nanoparticles (middle). (b) Detailed view on the high pressure region reveals reversible relaxation of such materials upon pressure release (see further investigations in Figure 4). *as published by Athanassiou et al.[60]

glycol molecules on the oxide surface of the particle has been assumed.[58] Thin films were made by spin-coating (1500 rpm, 42 s) the dispersions, resulting in a thickness of about 100 nm (Figure 1b) and a quite dense packing of nanoparticles (Figure 1c) after post-treatment of 550 °C for 10 min was observed. Nevertheless, some defects, as small cracks and shallow pits, are introduced in the film during the post treatment and show how volume loss due to surfactant removal may result in film imperfections.

Electrical Resistivity in the Presence of Insulating Shells. To correlate electrical resistivity to impurities and/or formation of insulating shells on the particles, we measured the organic impurity content from drying the organic molecule-coated particles (i.e., stabilized suspensions) after centrifugation and supernatant removal in vacuum at 60 °C. Because pressure-dependent resistivity measurements provide a more detailed insight into governing conduction mechanism in assembled nanoparticles, pills were pressed using the slightly prepestled powder (breaking the centrifugation pellets manually). Pills with systematically increasing organic shells around the ATO particles were prepared from the original dispersions based on ethylene glycol (EG, smallest molecule, less than 0.6 nm), trioxadecanoic acid (TODA, about the size of a fatty acid, 1−2 nm long) and polymeric dispersion additives (size above 2 nm; see subsequent sections for characterization). Figure 2 shows how the resistivity of pure ATO pills drops upon increasing pressure (from little load applied on the pill and a pressure of less than 1×10^1 bar to around 1×10^4 bar). Mechanical relaxation (irreversible or reversible nanoparticle compaction during these experiments) was investigated by releasing the pressure after applying the maximum pressure (10^4 bar) back to 10^3 bar and showed no relaxation for pure ATO samples (i.e., no insulating shells). A similar behavior was found for the thin organic layer coated samples derived from ATO coated/stabilized with the trioxadecanoic acid (TODA) and ethylene glycol (EG). These samples irreversibly compact (see Figure 2 b, insert).

In contrast, polymer dispersant-stabilized/coated ATO nanoparticle derived samples showed a reversible mechanical relaxation and resistance came back to initial values upon pressure reduction (see Figure 3b). We repeated the measurements for a number of times applying pressure cycles between 0.8 kbar (1 t) and 5.9 kbar (7.5 t). Multiple cycles (see Figure 4 for 5 consecutive compression/expansion cycles) clearly demonstrate reversible behavior, thus excluding irreversible compaction events as a cause of the here discussed effects. However, a minor drift in resistance is observed, which may be an effect of charge accumulation and discharging of single-nanoparticles working as capacitors in the composite as proposed by Oldfield et al.[59] An equilibrium state was generally reached after 3 h (no more drift). Using such long time equilibration conditions afforded a drift-free, constant, and

dx.doi.org/10.1021/am300319r | ACS Appl. Mater. Interfaces 2012, 4, 2664−2671

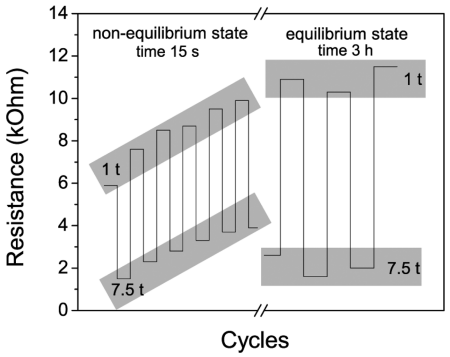

Figure 4. Cycles of 1 and 7.5 t (0.8−5.9 kbar) pressure applied to the polymer coated ATO pill show a reversible behavior of the resistance over more than 5 cycles. A drift in resistance is observed, but measurements after 3 h (equilibrium reached) showed the same behavior over more than 3 cycles. Therefore, the polymer/ATO samples fully relax after releasing pressure.

reversible behavior as demonstrated over 3 additional cycles (Figure 4). The polymer/ATO samples can, therefore, be considered to be noncompacting and fully relaxed after releasing pressure (Figure 3b).

Origin of Pressure-Dependent Resistivity in Core/Shell Composites. Pressure-dependent changes in electrical resistivity may originate from several effects: The piezoresistance may be explained by formation of a higher number of percolation paths through a pill (or any assembly of nanoparticles) as a result of powder compaction and denser packing.[61] Alternatively, the organic molecules forming the insulating shell are mobile and subsequent shell deformation and displacement increases the contact area between the conducting particle cores improving conductivity. Another possibility is that the electron transport through the insulating shells is not negligible and depends on the detailed molecular composition. The last possibility has been originally described by Athanassiou et al.[60] as altered electron tunneling through nanometer thick insulating shells as a result of shell compression during pressure load (i.e., shorter tunneling path and higher tunneling probability, thus smaller resistivity).

Do Insulating Surfactant Layers Behave Like Ceramic Shells? Assuming that the so far investigated organic shells are in principle nonconducting, we expect electron tunneling through the organic layer (EG, TODA surfactant or polymer). Shell displacement effects could be excluded based on above observation of reversible behavior (A) and by using a second, independent argument: Comparison of a rigid insulating shell (e.g., ceramic or silica shell) with a similar organic shell of the same thickness affords a similar piezoresistance. This was demonstrated by comparing the resistivity of compacted polymer/ATO composites to earlier investigations on ceramic-coated metal nanoparticles by Athanassiou et al.[60] (Figure 3 a).

To investigate the role of insulating shell thickness, we directly compared composites from ATO either with organic shells (EG, TODA, polymer) or silica for various layer thicknesses (Figure 5). The relative change in resistance as function of pressure is used to directly compare these two otherwise most different set of samples (for each material the resistance is normalized to the value at highest pressure, resistance at 7.5 t corresponds to 100%). At first, it becomes most evident that the organic shells show a more pronounced change in resistivity, which can be well understood if considering the much easier compaction of organic matter than silica (i.e., organic matter being much softer than silica). The behavior of the thinnest silica samples is best understood based on the absolute resistivity data given in Figure 6, which includes data for compaction and relaxation measurements (i.e., pressure was increased or decreased subsequently). For samples with no silica (see Supporting Information, Figure 3) or a very thin, possibly only partially coated layer[62] (nominal thickness of 0.7 nm silica), the materials irreversibly compacted similar to the previously discussed samples of ATO with no coating, EG or TODA surfactants. Less pronounced effects and overall greater resistance arise from increasing the silica layer thickness. A comparison of nominal shell thickness and optically measured values for the higher silica shells is given in Table 1.

A quantitative comparison using the tunneling formalism for such insulating shell/conducting core particles[60] affords a composite resistivity ρ as a function of pressure P as

$$\rho(P) = \rho_0 \exp(-2X_t d_0 P/M) \quad (1)$$

where d_0 is the mean distance between two particles (note that $d_0 = 2x$, where x is the shell thickness). M is the bulk

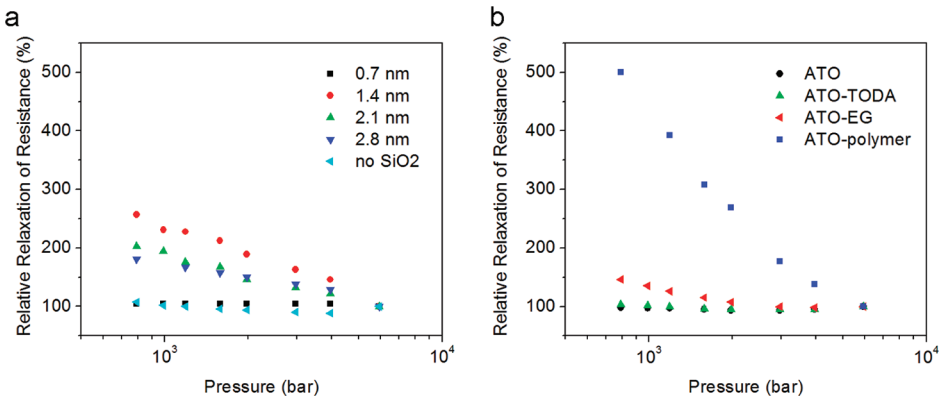

Figure 5. Relative changes in electrical resistance under elevated pressure for ATO samples with (a) increasing silica shell thickness allow a direct comparison of these samples. A thickness of around 1.4 nm results in the most pronounced piezoresistance (silica shells, left). (b) Organic material on the surface of conductor (ATO) nanoparticles provoked the same behavior: Small molecules (e.g., ethylene glycol) showed a similar pressure dependent resistance as low silica samples and polymeric shells (a few nm thick) afforded a stronger piezoresistance, similar to intermediate silica layers.

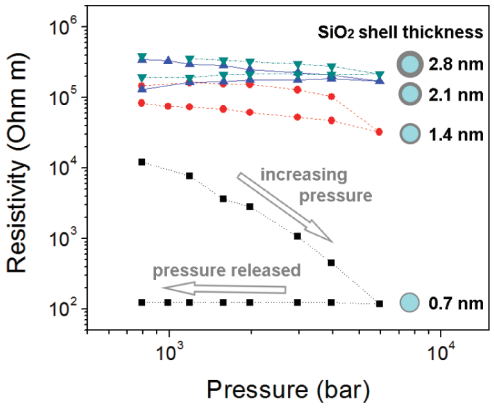

Figure 6. Layers of silica (a well-known insulator), increasing in thickness, were deposited in situ on conductor particles of ATO and resulted in a successively increased resistivity. Although very thin layers (0.7 nm) behaved similarly to pure ATO upon pressure release (irreversible compaction), the higher barrier samples (>2 nm silica) showed a less pronounced piezoresistance and partially relaxed upon pressure release.

compressive modulus of the coating material and X_t is defined as $X_t = (8\pi^2 m_{eff} V/h^2)^{1/2}$ with m_{eff} as the effective electron mass, V the potential barrier height at the material junction and h the Planck constant. The same exponential behavior of resistivity and conductivity for small biases is described by Zabet-Khosousi and Dhirani[42] for metal−insulator−metal junctions. For organic composites, polymer science describes piezoresistive behavior in the context of flexible sensors, where the pressure dependence of resistance is described as:[63]

$$\frac{R(P)}{R_0} = \frac{d}{d_0}\exp(-2X_t(d_0 - d)) = (1 - P/M)\exp(-2X_t d_0 P/M) \quad (2)$$

with $d = d_0(1 - P/M)$ and the resistance R. R_0 is the resistance measured at a given reference pressure. The expression R/R_0 is similar to ρ/ρ_0 as long as the pill thickness is not largely affected by compaction. For amorphous SiO_2 (bulk compressive modulus =36.9 GPa), P/M is very small in the pressure range of 1×10^3 to 1×10^4 bar and therefore the pre-exponential factor in eq 2 $(1-P/M)$ is nearly 1. Therefore, the two models are congruent in this case. For an assumed electron mass of $0.39 \cdot m_0$[64] and a potential barrier of 3.9 eV at the transition from ATO to amorphous SiO_2,[65,66] we can evaluate the present data (e.g., the nominal 1.4 nm SiO_2 shell sample) using eq 1. The data in Figure 7a shows a good qualitative match of the purely physical models (calculated data) and the experimental findings. The calculations yield a shell thickness of 2 nm. This is in the same size range than the experimentally observed shell thickness using electron microscopy images, where we found a mean shell thickness of 1.7 nm.

Note that above formalism assumes measurement at a small, constant applied voltage. The experiments performed here, however, were done at constant current and afforded voltage variations in a range of 10^{-1} to 10^0 V with peak values below 1.6 V. As the energy of these electrons is still significantly smaller than the potential barrier of 3.9 eV,[65,66] the tunneling phenomena above is not significantly suppressed. We measured the resistance at different applied voltages, and could clearly see the influence of the tunneling effect at voltages below the potential barrier, and the suppression of the effect above the barrier (see the Supporting Information, Figure 4). To quantitatively estimate the maximum deviations arising from this mode of measurement, we rerun the above calculations at a reduced barrier height of 2.3 eV (i.e., using 3.9 − 1.6 eV, the most extreme potential effects that may have arisen from choosing this type of measurement method) which afforded only minor changes in the resulting shell thickness (less than 30%). We can therefore still use the above model to qualitatively describe our systems (inorganic and organic shells).

Comparing the polymer/ATO composite to the recently reported metal/ceramic core/shell particles[60] again confirmed the observations made here in terms of reversibility and scaling of resistivity versus applied pressure (Figure 3). In the applied pressure range eq 1 and 2 are nearly congruent (see Figure 7b) for an assumed bulk modulus of 2 GPa of the investigated polymer (polyurethane copolymer with tertiary amine groups, information given by the supplier).[67,68]

CONCLUSION

This study shows the strong influence of nonconducting surface impurities introduced during the preparation of conductive nanoparticle films in a quantitative way and relates the experimental observations to a quantitative understanding based on an electron tunneling mechanism. The direct comparison of resistivity behavior of assemblies made from

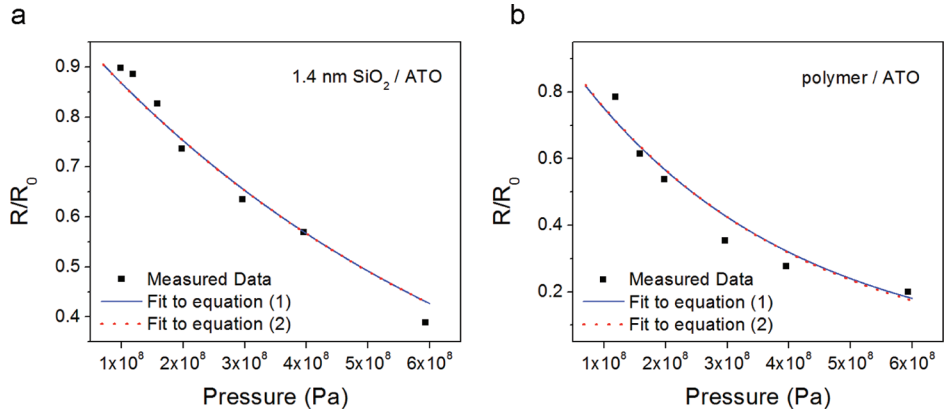

Figure 7. Evaluation of congruence of experimental data to theoretical models by fitting eq 1 and 2 to the measured data from (a) 1.4 nm SiO_2 on ATO particles and (b) polymer-coated ATO particles. The models show a good agreement for inorganic coated as well as organically coated ATO.

dx.doi.org/10.1021/am300319r | ACS Appl. Mater. Interfaces 2012, 4, 2664−2671

hard shell ceramics (e.g., silica) on conducting nanoparticles (metals or ATO) with commonly used organic surfactants in the preparation of conductive thin films demonstrates the identical influence of such nonconducting materials, even at minor concentrations. Large surfactant molecules (polymer) display comparable pressure dependent electron tunneling to 2 nm thick SiO_2 layers, whereas smaller molecules behave like assemblies of naked conducting nanoparticles. Understanding the role of surfactants, adsorbates or processing aids in thin film preparation will assist the development of improved film preparation methods as urgently required in photovoltaics and classical electronics.

■ ASSOCIATED CONTENT

Supporting Information

Results of thermogravimetrical analysis of organically coated ATO-nanoparticles (Supporting Figure 1); scheme of polymer−nanoparticle composite models (Supporting Figure 2); pressure-dependent resistivity measurement including non-SiO_2 coated ATO particles from same flame spray setup (Supporting Figure 3); resistance of 1.4 nm SiO_2 coated nanoparticles (under 1 t pressure) at different applied voltages (Supporting Figure 4). This material is available free of charge via the Internet at http://pubs.acs.org.

■ AUTHOR INFORMATION

Corresponding Author

*E-mail: wendelin.stark@chem.ethz.ch.

Notes

The authors declare no competing financial interest.

■ ACKNOWLEDGMENTS

The authors thank Frank Krumeich for performing transmission electron microscopy at the EMEZ (Electron Microscopy ETH Zurich) and Prof. Sotiris E. Pratsinis for useful discussions and for providing access to the enclosed flame spray pyrolysis reactor. Financial support from the ICB/ETHZ, Swiss National Science Foundation (Grant 200020-126694) and the European Research Council is kindly acknowledged.

■ REFERENCES

(1) Fortunato, E.; Ginley, D.; Hosono, H.; Paine, D. C. *MRS Bull.* **2007**, *32*, 242−247.
(2) Chopra, K. L.; Major, S.; Pandya, D. K. *Thin Solid Films* **1983**, *102*, 1−46.
(3) Ginley, D. S.; Bright, C. *MRS Bull.* **2000**, *25*, 15−18.
(4) Gordon, R. G. *MRS Bull.* **2000**, *25*, 52−57.
(5) Li, N.; Meng, Q. Synthesis and characterization of antimony-doped tin oxide (ATO) and its application in near infrared shielding glass paint. In *Proceedings of the International Conference on Advances in Energy Engineering 2010*; Beijing ; IEEE: Piscataway, NJ, 2010.
(6) Dawar, A.; Joshi, J. *J. Mater. Sci.* **1984**, *19*, 1−23.
(7) Minami, T. *Semicond. Sci. Technol.* **2005**, *20*, S35−S44.
(8) Murdoch, G.; Hinds, S.; Sargent, E.; Tsang, S.; Mordoukhovski, L.; Lu, Z. *Appl. Phys. Lett.* **2009**, *94*, 213301.
(9) Montero, J.; Herrero, J.; Guillén, C. *Sol. Energy Mater. Sol. Cells* **2010**, *94*, 612−616.
(10) Cui, J.; Wang, A.; Edleman, N. L.; Ni, J.; Lee, P.; Armstrong, N. R.; Marks, T. J. *Adv. Mater.* **2001**, *13*, 1476−1480.
(11) Mishra, K.; Johnson, K.; Schmidt, P. *Phys. Rev. B* **1995**, *51*, 13972.
(12) Chin, H. S.; Cheong, K. Y.; Razak, K. A. *J. Mater. Sci.* **2010**, *45*, 5993−6008.
(13) Hou, K.; Puzzo, D.; Helander, M. G.; Lo, S. S.; Bonifacio, L. D.; Wang, W.; Lu, Z. H.; Scholes, G. D.; Ozin, G. A. *Adv. Mater.* **2009**, *21*, 2492−2496.
(14) Look, D. C. *Mater. Sci. Eng., B* **2001**, *80*, 383−387.
(15) *Handbook of Photovoltaic Science and Engineering*; Luque, A., Hegedus, S., Eds.; John Wiley & Sons,: Chichester, U.K., 2011.
(16) Klein, A.; Koerber, C.; Wachau, A.; Saeuberlich, F.; Gassenbauer, Y.; Schafranek, R.; Harvey, S.; Mason, T. *Thin Solid Films* **2009**, *518*, 1197−1203.
(17) Lee, S. U. K.; Hong, B.; Boo, J. *World* **2010**, *3*, 119−123.
(18) Shanthi, E.; Dutta, V.; Banerjee, A.; Chopra, K. *J. Appl. Phys.* **1980**, *51*, 6243−6251.
(19) Coakley, K. M.; McGehee, M. D. *Chem. Mater.* **2004**, *16*, 4533−4542.
(20) Forrest, S. R. *Nature* **2004**, *428*, 911−918.
(21) Gustafsson, G.; Cao, Y.; Treacy, G. M.; Klavetter, F.; Colaneri, N.; Heeger, A. J. *Nature* **1992**, *357*, 477−479.
(22) Kim, M. G.; Kanatzidis, M. G.; Facchetti, A.; Marks, T. J. *Nat. Mater.* **2011**, *10*, 382−388.
(23) Buhler, G.; Tholmann, D.; Feldmann, C. *Adv. Mater.* **2007**, *19*, 2224−2227.
(24) Lee, S. U.; Boo, J. H.; Hong, B. *Jpn. J. Appl. Phys.* **2011**, *50*, 01AB10.
(25) Goebbert, C.; Nonninger, R.; Aegerter, M. A.; Schmidt, H. *Thin Solid Films* **1999**, *351*, 79−84.
(26) Mueller, V.; Rasp, M.; Rathouský, J.; Schütz, B.; Niederberger, M.; Fattakhova-Rohlfing, D. *Small* **2010**, *6*, 633−637.
(27) Van Bommel, M.; Groen, W.; Van Hal, H.; Keur, W.; Bernards, T. *J. Mater. Sci.* **1999**, *34*, 4803−4809.
(28) Hoertz, P. G.; Chen, Z.; Kent, C. A.; Meyer, T. J. *Inorg. Chem.* **2010**, *49*, 8179−8181.
(29) Al-Dahoudi, N.; Aegerter, M. A. *Thin Solid Films* **2006**, *502*, 193−197.
(30) Reindl, A.; Mahajeri, M.; Hanft, J.; Peukert, W. *Thin Solid Films* **2009**, *517*, 1624−1629.
(31) Cho, Y. S.; Kim, H. M.; Hong, J. J.; Yi, G. R.; Jang, S. H.; Yang, S. M. *Colloids Surf., A* **2009**, *336*, 88−98.
(32) Mahajeri, M.; Voigt, M.; Klupp Taylor, R.; Reindl, A.; Peukert, W. *Thin Solid Films* **2010**, *518*, 3373−3381.
(33) Koeniger, T.; Muenstedt, H. *J. Mater. Sci.* **2009**, *44*, 2736−2742.
(34) Talapin, D. V.; Lee, J. S.; Kovalenko, M. V.; Shevchenko, E. V. *Chem. Rev.* **2010**, *110*, 389−458.
(35) Maksimenko, I.; Gross, M.; Koeniger, T.; Muenstedt, H.; Wellmann, P. J. *Thin Solid Films* **2010**, *518*, 2910−2915.
(36) Krueger, S.; Hickey, S. G.; Tscharntke, S.; Eychmueller, A. *J. Phys. Chem. C* **2011**, *115*, 13047−13055.
(37) Mueller, K. H.; Herrmann, J.; Raguse, B.; Baxter, G.; Reda, T. *Phys. Rev. B* **2002**, *66*, 075417.
(38) Zamborini, F. P.; Leopold, M. C.; Hicks, J. F.; Kulesza, P. J.; Malik, M. A.; Murray, R. W. *J. Am. Chem. Soc.* **2002**, *124*, 8958−8964.
(39) Kleinjan, W.; Brokken-Zijp, J.; van de Belt, R.; Chen, Z.; de With, G. *J. Mater. Res.* **2008**, *23*, 869−880.
(40) Carotenuto, G.; Valente, M.; Sciume, G.; Valente, T.; Pepe, G.; Ruotolo, A.; Nicolais, L. *J. Mater. Sci.* **2006**, *41*, 5587−5592.
(41) Adams, D. M.; Brus, L.; Chidsey, C. E. D.; Creager, S.; Creutz, C.; Kagan, C. R.; Kamat, P. V.; Lieberman, M.; Lindsay, S.; Marcus, R. A.; Metzger, R. M.; Michel-Beyerle, M. E.; Miller, J. R.; Newton, M. D.; Rolison, D. R.; Sankey, O.; Schanze, K. S.; Yardley, J.; Zhu, X. Y. *J. Phys. Chem. B* **2003**, *107*, 6668−6697.
(42) Zabet-Khosousi, A.; Dhirani, A. A. *Chem. Rev.* **2008**, *108*, 4072−4124.
(43) Stark, W. J.; Strobel, R.; Guenther, D.; Pratsinis, S. E.; Baiker, A. *J. Mater. Chem.* **2002**, *12*, 3620−3625.
(44) Teleki, A.; Suter, M.; Kidambi, P. R.; Ergeneman, O.; Krumeich, F.; Nelson, B. J.; Pratsinis, S. E. *Chem. Mater.* **2009**, *21*, 2094−2100.
(45) Grass, R. N.; Stark, W. J. *J. Mater. Chem.* **2006**, *16*, 1825−1830.
(46) Stark, W. J.; Maedler, L.; Maciejewski, M.; Pratsinis, S. E.; Baiker, A. *Chem. Commun.* **2003**, 588−589.

(47) Maedler, L.; Kammler, H. K.; Mueller, R.; Pratsinis, S. E. *J. Aerosol Sci.* **2002**, *33*, 369−389.
(48) Teleki, A.; Heine, M. C.; Krumeich, F.; Akhtar, M. K.; Pratsinis, S. E. *Langmuir* **2008**, *24*, 12553−12558.
(49) Borchert, H.; Shevehenko, E. V.; Robert, A.; Mekis, I.; Kornowski, A.; Grubel, G.; Weller, H. *Langmuir* **2005**, *21*, 1931−1936.
(50) Melzak, K. A.; Sherwood, C. S.; Turner, R. F. B.; Haynes, C. A. *J. Colloid Interface Sci.* **1996**, *181*, 635−644.
(51) Fleer, G. J.; Cohen Stuart, M. A.; Scheutjens, J. M. H. M.; Cosgrove, T.; Vincent, B. *Polymers at Interfaces*; Chapman & Hall: London, 1993.
(52) *Perry's Chemical Engineers' Handbook*, 7th ed.; Perry, R. H., Green, D. W., Eds.; The McGraw-Hill Companies: New York, 1997.
(53) Athanassiou, E. K.; Grass, R. N.; Stark, W. J. *Aerosol Sci. Technol.* **2010**, *44*, 161−172.
(54) Pratsinis, S. E. *Prog. Energy Combust. Sci.* **1998**, *24*, 197−219.
(55) Stark, W. J.; Pratsinis, S. E. *Powder Technol.* **2002**, *126*, 103−108.
(56) Teleki, A.; Akhtar, M. K.; Pratsinis, S. E. *J. Mater. Chem.* **2008**, *18*, 3547−3555.
(57) *Colloid Science: Principles, Methods and Applications*, 2nd ed.; Cosgrove, T., Ed.; John Wiley & Sons: Chichester, U.K., 2010.
(58) Zhao, J.; Tan, R.; Zhang, Y.; Yang, Y.; Guo, Y.; Zhang, X.; Wang, W.; Song, W. *J. Am. Ceram. Soc.* **2011**, *94*, 725−728.
(59) Oldfield, G.; Ung, T.; Mulvaney, P. *Adv. Mater.* **2000**, *12*, 1519−1522.
(60) Athanassiou, E. K.; Krumeich, F.; Grass, R. N.; Stark, W. J. *Phys. Rev. Lett.* **2008**, *101*, 166804.
(61) Mamunya, Y. P.; Zois, H.; Apekis, L.; Lebedev, E. V. *Powder Technol.* **2004**, *140*, 49−55.
(62) Sotiriou, G. A.; Sannomiya, T.; Teleki, A.; Krumeich, F.; Voeroes, J.; Pratsinis, S. E. *Adv. Funct. Mat* **2010**, *20*, 4250−4257.
(63) Zhang, X. W.; Pan, Y.; Zheng, Q.; Yi, X. S. *J. Polym. Sci., Part B* **2000**, *38*, 2739−2749.
(64) Schenk, A.; Heiser, G. *J. Appl. Phys.* **1997**, *81*, 7900−7908.
(65) DiStefano, T.; Eastman, D. *Solid State Commun.* **1971**, *9*, 2259−2261.
(66) Guzman, G.; Dahmani, B.; Puetz, J.; Aegerter, M. A. *Thin Solid Films* **2006**, *502*, 281−285.
(67) Goldberg, A. J.; Craig, R. G.; Filisko, F. E. *J. Dent. Res.* **1978**, *57*, 563−569.
(68) Mott, P. H.; Roland, C. M.; Corsaro, R. D. *J. Acoust. Soc. Am.* **2002**, *111*, 1782−1790.